

APPLICATION OF SCANNING ELECTRON-ACOUSTIC MICROSCOPY TO BIOLOGICAL MATERIALS ¹

Chun-ming Gao² Shu-yi Zhang^{2,3} Peng-cheng Miao² Zhong-ning Zhang² and Ting Yu²

Lab of Modern Acoustics, Institute of Acoustics, Nanjing University, Nanjing 210093,

China

ABSTRACT

The imaging methods and results of biological materials by scanning electron acoustic microscopy (SEAM) have been introduced in this paper. The images of amplitude and phase of plant leaf by SEAM show that the amplitude image involves more surface features but the phase image displays more subsurface structures. The laminated imaging experiments, which use the x- and y- components of SEAM signals with different reference phases, show the subsurface structures in different depths of biological materials, such as, plant leaves, biological tissues and etc. Using a photothermal technique, the thermal diffusion lengths of the samples of biological materials can be evaluated, by which the depths of the subsurface structures in the laminated images can be estimated. In addition the damage areas of the leaf and muscles are also imaged by SEAM. For comparison, the second electron images of the same areas of the samples studied by SEAM are also obtained. The images show that the SEAM is sensitive to micro-structures of surface and also subsurface structures of biological materials.

Keywords: Biological materials; Electron-acoustic microscopy; Laminated imaging; Subsurface structure;

1. INTRODUCTION

Scanning electron-acoustic microscopy (SEAM) has been widely used for imaging and analyzing of many kinds of non-biological materials ^[1-5], specially for biomedical materials ^[3,5]. Based on the principle of laminated imaging of the photoacoustic thermal wave microscopy ^[6], a laminated imaging system of SEAM has been established ^[7]. The spacial resolution and the signal to noise ratio are improved by enhancing the intensity and the modularity of the electron beam. As we have known, the amplitude images show mainly surface topographs and the phase images show the subsurface structures. In phase images, some configurations in the subsurface cannot be seen in the amplitude images. The images obtained at different modulation frequencies involve the structures in different depth ranges of the samples. On the other hand, the imaging by x or y component of the SEAM signals with different reference phases shows the structures at different depths of the samples. By

frequency and phase adjusting of SEAM, the laminated imaging experiments have been successfully performed for several materials and structures, such as, integrated circuits with submicron structures, ferroelectric domains of PZT, crystal shapes of metals, depth distributions of residual stress in aluminum alloys indented by a micro-indenter or induced by a high intensity laser beam, and etc., which display the SEAM system is very sensitive and available.

Then, the system is used for analyzing some biological materials, such as, leaves of plants, tissues of liver, heart, muscle of rats and cornea of human. The micro-structures, such as, muscle fibers, blood vessels, voids and others are shown clearly in SEAM laminated images. In addition, damage experiments of biological tissues have also been done, in which the damaged area impinged by an electron beam or laser beam is very clearly displayed in scanning electron-acoustic (SEA) images. In order to comparison with the secondary electron (SE) images of the same samples are also obtained. It is shown that the subsurface structures or damaged areas of the samples almost cannot be seen in SE images.

2. METHODS

The experimental system of SEAM is a modified scanning electron microscope, in which the electron beam is intensity-modulated at frequency f and focused on the sample. The local periodic heating of the sample surface produces a thermal wave and then an acoustic wave. The solution of the heat diffusion equation shows that the thermal diffusion length μ_t is expressed as ^[6]:

$$\mu_t = \sqrt{\frac{K}{\pi f \rho C}} \quad (1)$$

where K, ρ, C are the thermal conductivity, density and specific heat of the sample, respectively. But the thermal wave is so highly damped that typically propagates no more than a thermal diffusion length. The surface and subsurface features within μ_t of the sample may serve as scatterers during a thermal wave propagates, thus the acoustic signal will be generated as a result of thermal-to-acoustic mode conversion. A piezoelectric transducer (PZT) contacted tightly with the bottom of the sample converts the acoustic signals into electrical signals. In order to amplify the signals and suppress the noise, a preamplifier and then a lock-in amplifier are used, then the output of a PZT is amplified and mixed with a reference signal by the lock-in amplifier. The final imaging signal \bar{V} is ^[6]:

$$\bar{V} = \int_0^{x_m} |V(x')| \cos[\psi(x') - \psi_0] dx' \quad (2)$$

where x_m is the maximum penetration depth of the thermal wave, $V(x')$ and $\psi(x')$ are the output signal and the phase lag caused by the thermal source at point x' , ψ_0 is the

phase shift of the reference signal of the lock-in amplifier. The output signal \bar{V} reflects the structures of the sample in the thermal-wave penetration range.

It is possible to get different images by varying the frequency to display the properties and structures in different depth ranges because of the thermal diffusion length is inversely proportional to the square root of f . On the other hand, as the phase of the thermal source $\psi(x')$ is the same as the reference phase ψ_0 , the imaging signal approaches a maximum, i.e., the imaging signal contributed by the structure at x' can be strengthened by the lock-in amplifier. Thus the laminated imaging can be obtained by changing the reference phase.

In our SEAM, the electron beam can be modulated at the frequency range of 1KHz - 1MHz with an accelerated voltage 20KV - 30KV . The SEA signal is detected by PZT disks with different thicknesses, bonded to the bottom of the sample, and fed to a wideband preamplifier and then a lock-in amplifier with a bandwidth up to 1 MHz. Both amplitude and phase of the output of the lock-in amplifier can be acquired and processed by a computer. Finally, the amplitude A and phase ψ images of the SEA signal can be obtained and displayed in the monitor of the computer. Meanwhile, the images corresponding to x component $A \cos(\psi - \psi_0)$ and y component $A \sin(\psi - \psi_0)$ of SEA signal can also be got by the lock-in amplifier and displayed in the monitor. The x component and y component images show two different structures at different depths of the sample, in which the detected depth depends on the reference phase ψ_0 . By changing the reference phase, the laminated images with different depths can be obtained. On the other hand, the SE image can be obtained in the same area of the sample for comparison.

3. EXPERIMENTAL RESULTS AND DISCUSSIONS

3.1 Preparation and thermal characters of biological samples

The samples with the thickness about 1mm are prepared as usual as for scanning electron microscopy. For biological materials, the processes are five steps:

(1) Cleaning the samples with saline solution; (2) fixing the samples with glutaraldehyde and osmium tetroxide solutions; (3) dehydrating the samples gradually with acetone; (4) evaporating the residual water in the samples with a critical-point dryer; (5) plating very thin gold film on the surface of the samples.

In order to evaluate the imaging depth (d), the thermal diffusion length μ_t is measured by a photothermal technique, the thermal diffusion length of the biological samples are about in the range of $10\mu\text{m}$ to $20\mu\text{m}$ when the modulation frequency is 200KHz .

3.2 Amplitude image and phase image of phoenix leaf

Fig.1 shows the images of a phoenix leaf: a, the SE image, b, the SEA images at the modulation frequency of 184KHz: (1) amplitude image and (2) phase image. Many netted veins structures and gas holes at the surface are showed clearly in SE image (Fig.1a). The amplitude image of the SEAM in Fig.1b(1) is similar to the SE image, but the microstructures are less clear, which means the amplitude imaging of the SEAM is with lower resolution than that of the SE imaging for the leaf due to the influence of some subsurface structures. The phase image in Fig.1b(2) just shows a few structures, which means the phase image is not sensitive to the surface structures, but may involve mainly the information of the subsurface structures.

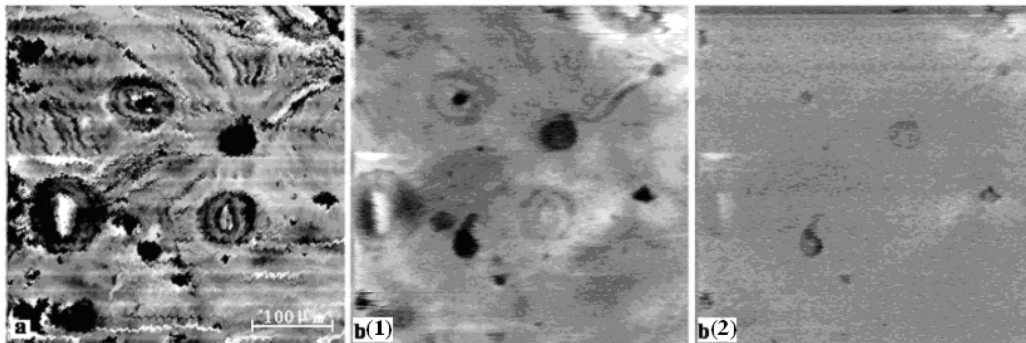


Fig.1 Images of phoenix leaf: a, SE image; b, SEA images at $f=184\text{KHz}$: (1) amplitude image; (2) phase image

3.3 Laminated imaging of biological tissues

At first, the SE images of the plant leaf and medical tissues are obtained for comparison. Then the imaging experiments of x components of SEA signals are carried out with different reference phases. In these experiments, some laminated images of the subsurface structures in different depths are displayed in the SEA images, which are not showed in the SE images.

3.3.1 Laminated imaging of loquat leaf

A SE image and five SEA images of a loquat leaf are showed in Fig.2. The netted veins, fibers and holes are showed clearly in the SE image, but only the holes are showed in the SEA laminated images. In addition, comparing the images from Fig.2b(1) to (5), the size of the hole A becomes smaller with the phase increases, i.e., with the depth increases; for positions B and C, also some small structures change gradually with the depth varying.

Generally, using SEAM for plant tissues, more information of subsurface can be displayed without destructive incision.

3.3.2 laminated imaging of biomedical tissues

(1) Laminated imaging of cornea tissue of human:

A SE image and five SEA images of a human cornea are shown in Fig.3. In the SE image (Fig.3a) shows many micro-structures at the surface of the cornea, which

are not displayed clearly in the SEAM images. However, some varies of the subsurface structures with the depth are shown in Fig.3b(1)-(5), such as, a funnel like structure in position A is showed outstandingly in all images of Fig.3b. Comparing the five SEA images, the size of the funnel ventage increases from Fig.3b(1) to Fig.3b(4) and then almost disappears in Fig.3b(5), which illustrates probably the related structures is almost located in the range of the imaging depth of Fig.3b(8). By evaluating the thermal diffusion length of the tissue, the depth of the funnel structure about $15\mu\text{m}$ is estimated. In addition, for position B, some structures in subsurface also change gradually from Fig.3b(1) to Fig.3b(5).

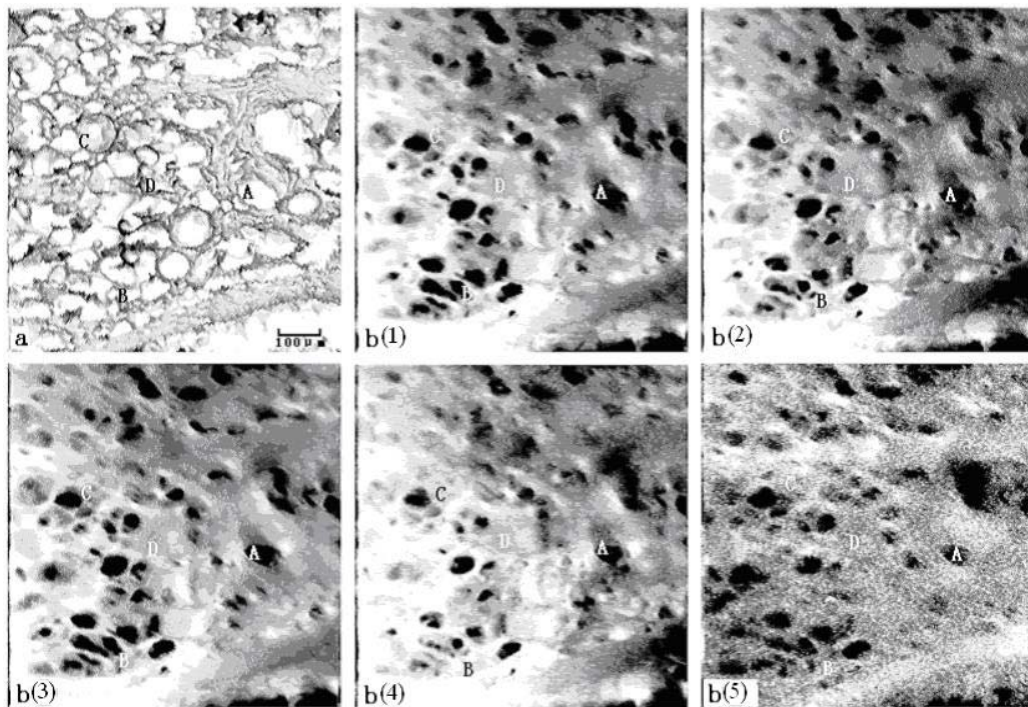


Fig.2 Images of a leaf tissues: a, SE image; b, SEA images at $f=200\text{KHz}$ and $\mu_t \approx 10\mu\text{ m}$: (1) $\theta = 20^\circ$, $d \approx 0.9\mu\text{ m}$; (2) $\theta = 60^\circ$, $d \approx 3.3\mu\text{ m}$; (3) $\theta = 100^\circ$, $d \approx 5.6\mu\text{ m}$; (4) $\theta = 140^\circ$, $d \approx 7.8\mu\text{ m}$; (5) $\theta = 180^\circ$, $d \approx 10\mu\text{ m}$.

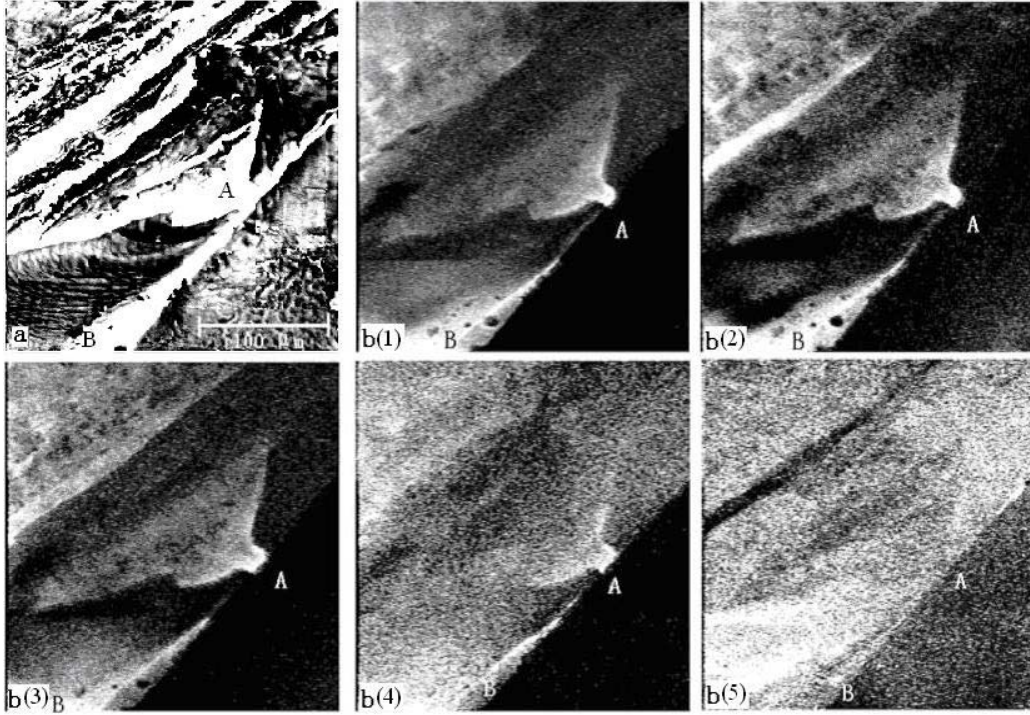


Fig.3 Images of a human cornea: a, SE image; b, SEA images at $f=205\text{KHz}$ and $\mu \approx 15\mu\text{ m}$: (1) $\theta = 10^\circ$, $d \approx 0.84\mu\text{ m}$; (2) $\theta = 25^\circ$, $d \approx 2.09\mu\text{ m}$; (3) $\theta = 55^\circ$, $d \approx 4.59\mu\text{ m}$; (4) $\theta = 145^\circ$, $d \approx 12.1\mu\text{ m}$; (5) $\theta = 175^\circ$, $d \approx 14.6\mu\text{ m}$

(2) Laminated imaging of heart tissue of rat:

A SE image and three SEA images of envelope tissue of a rat heart are showed in Fig.4. In the SE image (Fig.4a), some netted structures are showed clearly. In the SEA images, the Fig.4b(1) is also a surface feature because of it almost the same as Fig.4a. For position A, a fiber-like structure becomes thinner and then break down from Fig.4b(1) to Fig.4b(4). For positions B, C and D, the micro-structures in Fig.4b(1)-(3) are also varying gradually from b(1) to b(4).

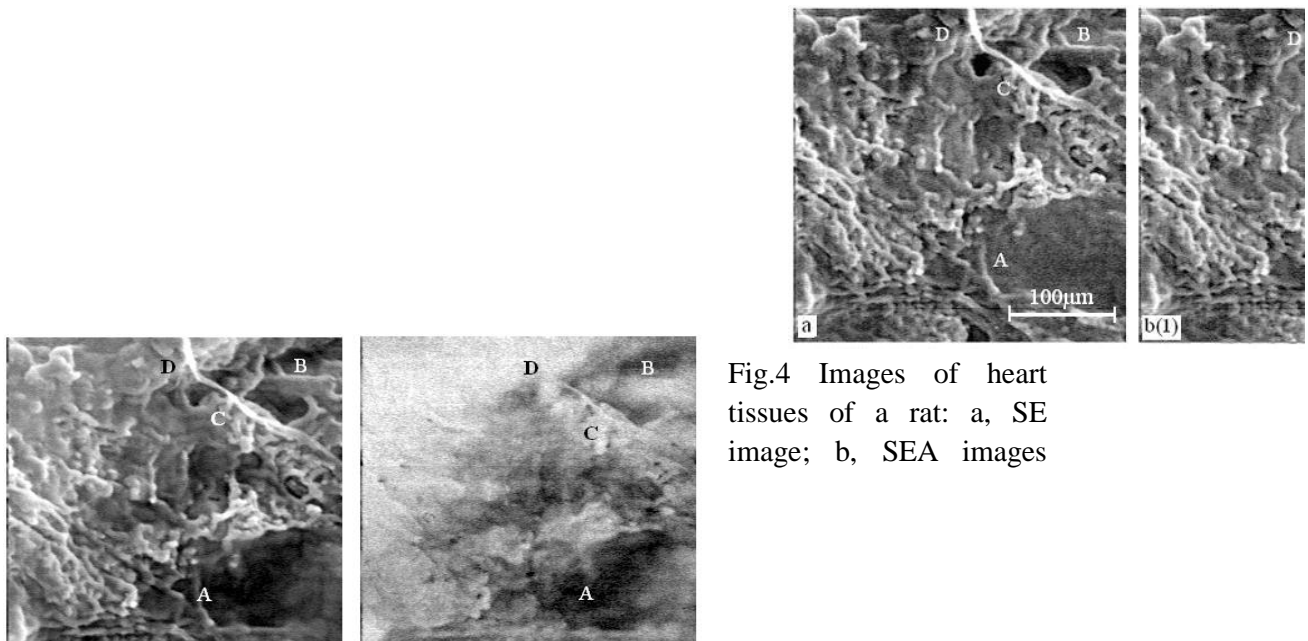


Fig.4 Images of heart tissues of a rat: a, SE image; b, SEA images

at $f=200\text{KHz}$ and $\mu \approx 20\mu\text{ m}$:

$$(1)\theta = 0^{\circ}, d \approx 0\mu\text{ m};$$

$$(2)\theta = 45^{\circ}, d \approx 5\mu\text{ m};$$

$$(3)\theta = 90^{\circ}, d \approx 10\mu\text{ m};$$

$$(4)\theta = 135^{\circ}, d \approx 15\mu\text{ m};$$

(3) Laminated imaging of liver tissue of rat:

A SE image and three SEA images of a rat liver are showed in Fig.5. A fistular structure is cross through the whole tissues from position A to positions B, C and D. The SE image (Fig.5a) shows the shape of the fistulae at the surface, which has different depths in different parts. From Fig.5b(1)-(3), the imaging depth approaches gradually to the same depth of the backside wall of the fistular structure, which is about $20\mu\text{ m}$. For position C, some small micro-structures also change from Fig.5b(1) to (3).

3.4 Damage of biological tissue

As we know the biological tissues are always damaged by laser beam (such as human skin or retina) or electron beam (samples in SEM). In this section, some damaged images are carried out.

(1) An electron beam with 30KV of SEM is used to irradiates a muscle tissue of rat for half an hour, then image the damaged areas by SEM and SEAM in Fig.6. Some muscle fibers are showed in both Fig.6a and Fig.6b, but the damage area as a square block is showed in SEA image (Fig.6b) only, not showed in SE image (Fig.6a).

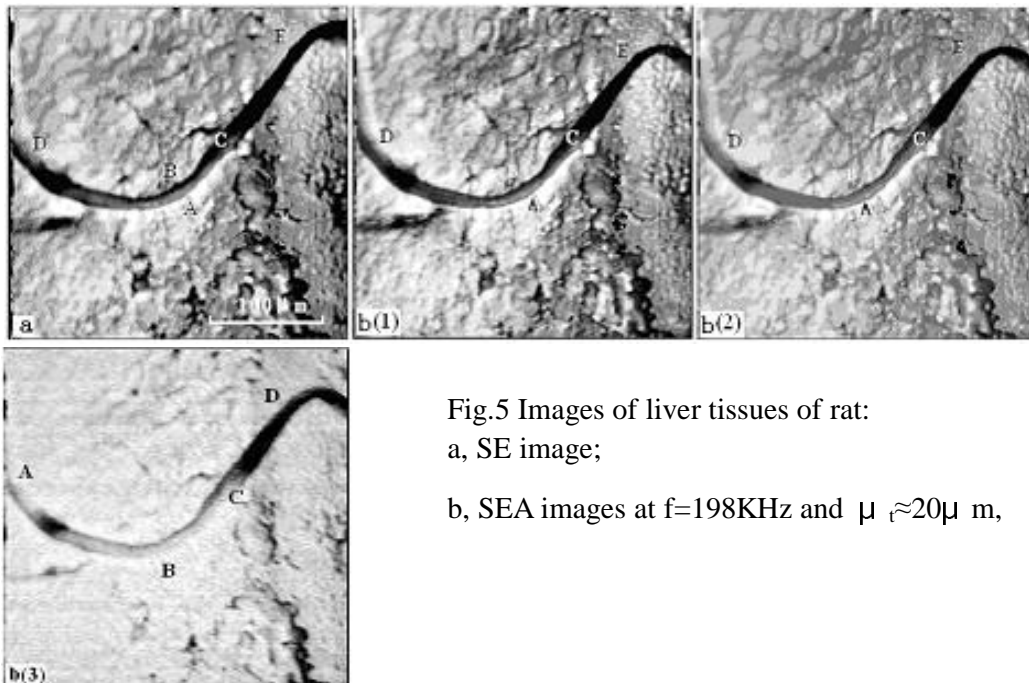


Fig.5 Images of liver tissues of rat:

a, SE image;

b, SEA images at $f=198\text{KHz}$ and $\mu \approx 20\mu\text{ m}$,

(1): $\theta = 0^{\circ}$, $d \approx 0\mu\text{ m}$;

(2): $\theta = 45^{\circ}$, $d \approx 5\mu\text{ m}$;

(3): $\theta = 135^{\circ}$, $d \approx 15\mu\text{ m}$;

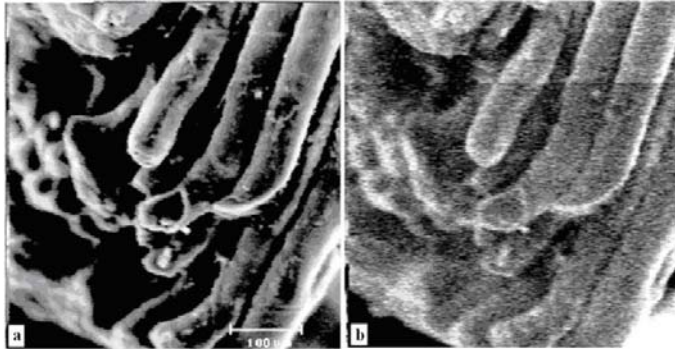


Fig.6 Images of muscle tissues of rat damaged by high energy electron beam irradiation:

a, SE image;

b, SEA amplitude image at $f=197\text{KHz}$.

Another damage experiment is carried out for a poplar leaf with the same method. The SE image (Fig.7a) shows the gas holes, nervations and cells on the surface clearly, but the SEA image shows also a square block of damaged area (Fig.7b).

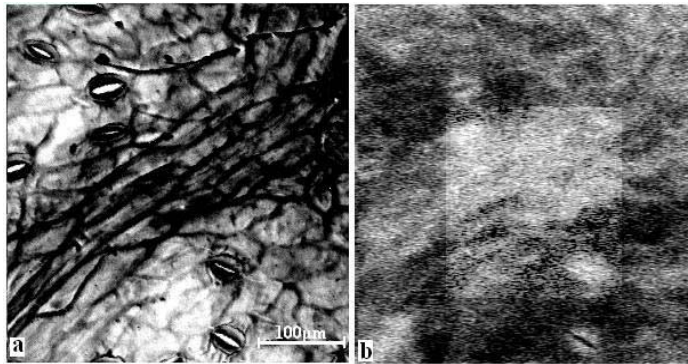


Fig.7 Images of a poplar leaf damaged by high energy electron beam irradiation:

a, SE image;

b, SEA amplitude image at $f=202\text{KHz}$.

(2) A laser beam is used to irradiate a loquat leaf, and the laser is so strong that a hole A is formed, which can be seen in Fig.8, meanwhile the neighbor area A' of the hole is withered. In the SEM picture (Fig.8a), it is difficult to distinguish the different A and A' areas, but it is easy to distinguish in SEAM picture (Fig.8b). For area B, which is slightly damaged, the different structures compared with other areas are showed in Fig.8b, but not in Fig.8a.

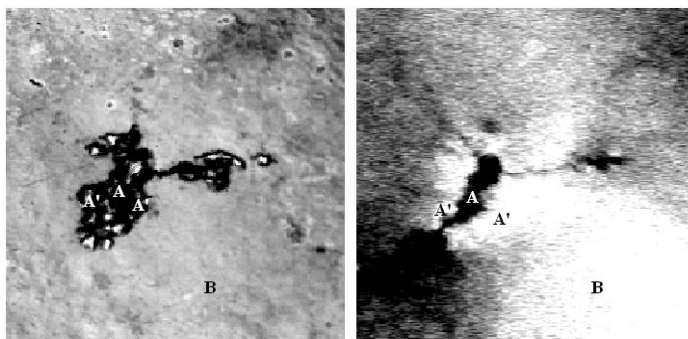


Fig.8 Images of a poplar leaf
damaged by a laser beam
irradiation:
a, SE image;
b, SEA amplitude image at $f=202\text{KHz}$.

4. CONCLUSIONS

From the SEM and SEAM imaging results and discussions for biological tissues, several conclusions can be obtained.

1, The SEAM established on the basis of SEM can be used to analyze the subsurface structures of the biological tissues.

2, Due to the thermal wave excited by electron beam has a limited penetration length, it is possible to get imaging of the subsurface structures of the samples. Based on the diffusion length is inversely proportional to the square root of the modulation frequency, the structure images in different depths can be obtained by changing the modulation frequency of the electron beam.

3, The signal of the SEAM is an integration of the signals contributed by the thermal wave sources distributed in the penetration length, the surface resolution of it is lower than that of the SEM for some tissues because of the influence of the subsurface structures.

4, Based on the signal produced by the thermal source (subsurface structure) in different depths has different phase lags, the laminated imaging of biological tissues can be obtained by adjusting the reference phase of the lock-in amplifier.

5, As the thermal penetration length of the biological tissues can be evaluated by a photothermal technique, the depth of the laminated imaging can also be estimated.

6, Generally, the SEAM can provide some special information on the subsurface structures of biological tissues, which cannot be obtained by SEM.

7, The imaging depths must be estimated further more precisely, which are in progress.

ACKNOWLEDGMENTS

This work is supported by National Natural Science Foundation of China, No. 10174038.

REFERENCES:

1. Cargill, III G S. *Nature*, 286: 691, (1980).
2. E. Brandis, A. Rosencwaig, *Appl. Phys. Lett.*, 37: 98, (1980).
3. L.J. Balk, M. Domnik and E. Bohm, *SPIE* 809, pp.219-224, (1987).
4. L.X. Liu, L.J. Balk, *Journal of Materials Science* 33, 4543-4549, (1998).
5. L.J. Balk, *Advanced Electronics and Electron Physics* 71, pp.1-73, (1988).
6. S. Y. Zhang, L. Chen, in *photoacoustic and thermal wave Phenomena in Semiconductors*, Ed., A. Mandelis (Elsevier Science Publishing co. Inc., 1987), pp. 27-52

7. Y. Hong, Z. N. Zhang, S. Y. Zhang, Z. Q. Li and X. J. Shui, 25th International Acoustical Imaging Symposium (March 19-22, 2000, Bristol, United Kingdom)
8. L. J. Balk, M. Domnik, K. Niklas, and P. Mestres, in Springer Series in Optical Sciences, Vol. 62, Photoacoustic and Photothermal Phenomena II, Eds: J. C. Murphy, J. W. MacLachlan-Spider and B. S. H. Royce, (Springer-Verlag, Berlin, 1990)